Electronic Supplementary Material (ESI) for ChemComm.

Supplementary Information

Capacity fade in high energy silicon-graphite electrodes for lithium-ion batteries

W. M. Dose[a], M. J. Piernas-Muñoz[a], V. A. Maroni[a], S. E. Trask[a], I. Bloom[a] and C. S. Johnson[a]

[a.] Chemical Sciences and Engineering Division, Argonne National Laboratory, Lemont, Illinois, U.S.A. 60439.

Experimental

Commercial $LiFePO_4$ (LFP) from Hydro Quebec was homogenously mixed with C-45 carbon conductive additive and polyvinylidene fluoride (PVdF) in a weight ratio of 90:5:5 and cast using N-methyl-2-pyrrolidone (NMP) as the solvent onto 20 μm thick Al current collector with a 7 MIL doctor blade. After drying the laminate at 75 °C overnight and then the punched electrodes at 75 °C under vacuum overnight, the active mass loading was 15.7 mg cm^{-2}. The Si-graphite electrode used in this study was obtained from the Cell Analysis Modeling and Prototyping (CAMP) facility at Argonne and is composed of commercially available materials. This electrode consists of Si (Nano&Amor, 50-70 nm), graphite (Hitachi Mage), C-45 carbon, and lithium polyacrylate (LiPAA) binder in a weight ratio of 73:15:2:10, respectively. Water was used as the solvent and the electrode was dried at 50 °C. After further drying the punched electrodes at 150 °C in a vacuum oven overnight the loading of the electrochemically active components (Si and graphite) was 0.7 mg cm^{-2}.

Electrochemical cells were assembled using 2032-type coin cells in an argon-filled glove box with < 1 ppm oxygen. The electrolyte (Gen2+10 % fluorethylene carbonate [FEC]) consists of 1.2 M $LiPF_6$ in ethylene carbonate: ethyl methyl carbonate, 3:7 wt/wt, with 10 wt. % of FEC. The Celgard separator was dried at 60 °C under vacuum prior to use. In half cell configuration, 15.6 mm diameter Li metal chips (MTI) were used as the reference/counter electrode. All electrochemical tests were performed using a MACCOR Series 4000 Test System at room temperature. The LFP/Si-graphite pseudo-full/reference cells were cycled from 2.0 to 3.4 V, with the upper potential cut-off determined from a capacity limited charge experiment. This ensured the $Li_{15}Si_4$ phase was not formed. The first and last three cycles of each set of 100 were conducted at a 0.047 mA cm^{-2} rate, or lithiation of the Si-graphite in a 10 h time period, C/10. The intermediate cycles (cycle 4-97) were conducted at different rates to understand the effect of current rate on the capacity fade. These were 0.047 mA cm^{-2}, 0.094 mA cm^{-2}, and 0.47 mA cm^{-2}, corresponding to approximately C/10, C/5 and C/1, respectively.

To investigate the morphology and structure of the Si-graphite electrode before and after electrochemical cycling scanning electron microscopy (SEM) and Raman spectroscopy were performed. The Si-graphite electrodes were harvested for characterisation using the following protocol. Full cells were disassembled inside an Ar filled glove box and the harvested electrodes washed twice with dimethyl carbonate (DMC) to remove excess electrolyte residue. Samples were transferred from the Ar filled glove box to the SEM in an airtight sample holder device. SEM images were recorded using a scanning electron microscope JEOL JSM6610LV equipped with a secondary electron detector (SED) and a backscattered electron detector (BSED). Topography and morphology of the samples were collected with the SED, while BSED allowed examination of the atomic number (Z) contrast. Elemental mapping analyses were conducted using the SEM (JEOL JSM6610LV) coupled to an energy dispersive X-ray spectroscopy (EDS) unit from Oxford Instruments (model 51-XMX1030), and the corresponding EDS data were analyzed with Aztec software. In all the cases, the scanning electron microscope was operated at 10 kV.

The Raman measurements were carried out using a Renishaw inVia Raman Microscope. Raman excitation was achieved with a 785 nm diode laser and the spectrum was scanned with a 1200 line mm^{-1} grating. The pristine and the cycled samples were placed in threaded Teflon sample holders (International Crystal Laboratories Micro Qik Cell/Part # 00006-2093) that incorporate rubber o-ring seals to prevent contact of the sample with ambient atmosphere. In this embodiment the electrode sample is pressed between a BaF_2 window (15 mm in diameter and 2 mm thick) and a stainless steel backing disk. Raman spectra were recorded through the BaF_2 window using a 50-X focusing/collection optic with a numerical aperture of 0.5. The excitation laser was brought to a focus at the sample/BaF_2 interface and the beam was expanded to a circular area approximately 10 μm in diameter. By performing this beam expansion and limiting the laser power delivered to the sample to < 4 mW, the effective laser power density present in all of the reported measurements was kept well below 1 mW μm^{-2}, i.e., well below the threshold we have established for laser damage to typical electrode samples. Spectra measured at individual spots typically consisted of a dozen or more 20 second acquisitions. The displayed spectra are an average of measurements at 25 separate spots on both pristine and cycled electrodes. The narrow, relatively weak BaF_2 phonon at 242 cm^{-1} provided both an internal frequency standard and a pseudo-intensity standard. All baseline corrections, intensity normalizations, and spectra averaging were performed with Wire 4.1 and GRAMS 32/AI software.

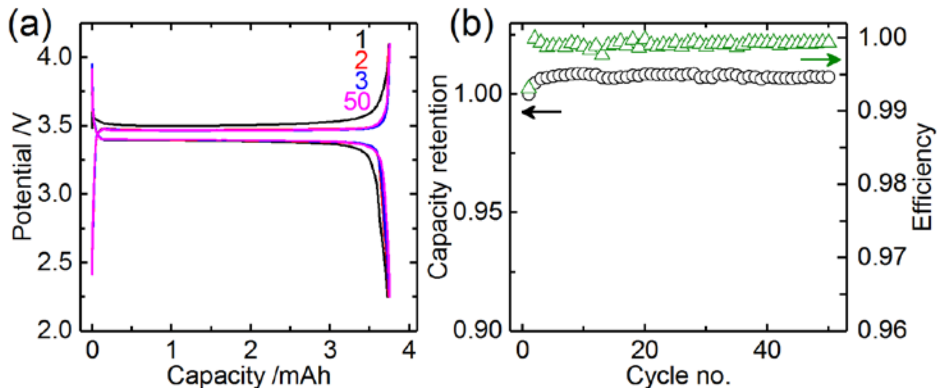

Fig. S1. Representative (a) electrochemical profile versus capacity with cycle number, and (b) capacity retention and cycle efficiency with cycle number of high capacity $LiFePO_4$ cycled against Li metal at C/10.

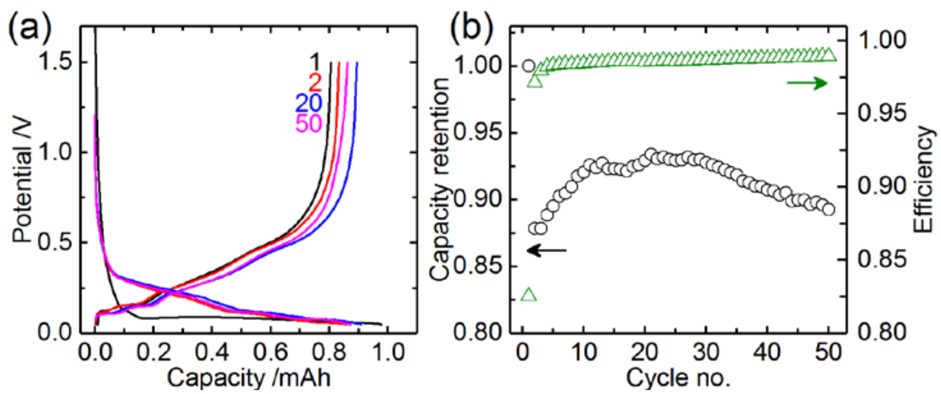

Fig. S2. Representative (a) electrochemical profile versus capacity with cycle number, and (b) capacity retention and cycle efficiency with cycle number of 15%Si-graphite cycled against Li metal at C/10.

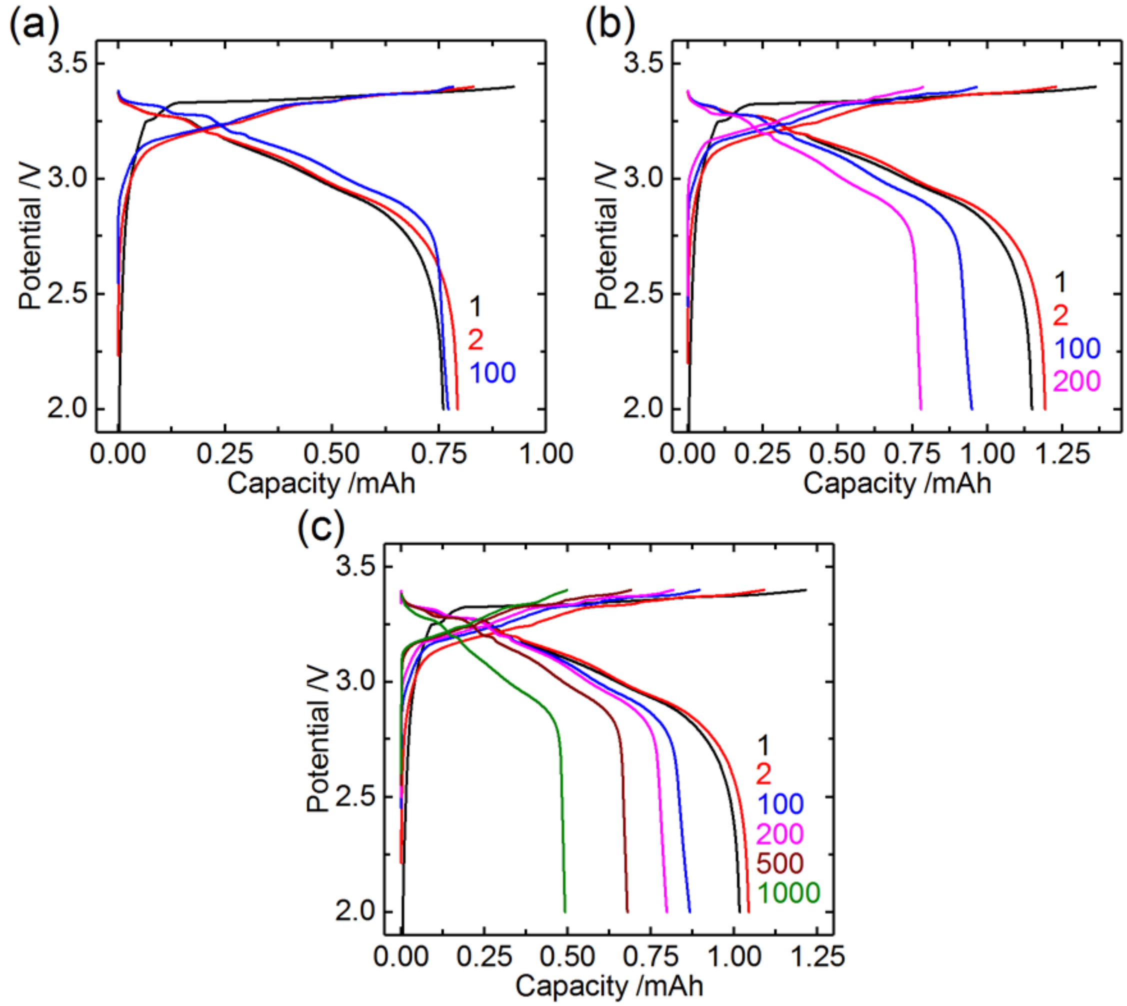

Fig. S3. Representative electrochemical profile versus capacity with cycle number of 15%Si-graphite cycled against a $LiFePO_4$ reference electrode at (a) C/10, (b) C/5, and (c) 1C. In (b) and (c) the first and last 3 cycles of each set of 100 cycles were performed at C/10 while the intermediate cycles were performed at C/5 and 1C, respectively. At C/10 100 cycles were collected, while 200 and 1000 cycles were collected at C/5 and 1C, respectively.

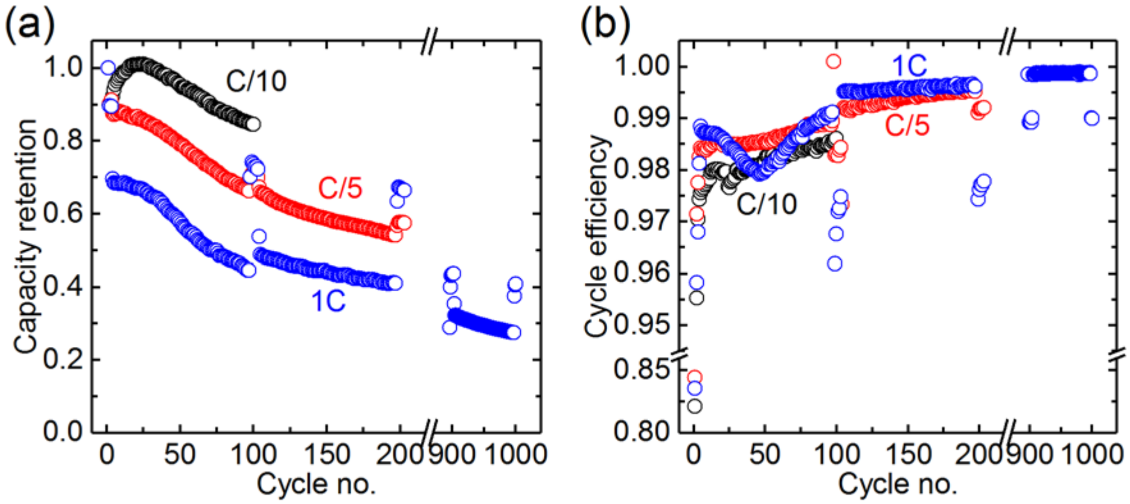

Fig. S4. Capacity retention (a) and cycle efficiency (b) with cycle number of 15%Si-graphite against a $LiFePO_4$ reference electrode. For the C/5 and 1C data, the first and last 3 cycles of each set of 100 cycles were performed at C/10 while the intermediate cycles were performed at C/5 and 1C, respectively. At C/10 100 cycles were collected, while 200 and 1000 cycles were collected at C/5 and 1C, respectively.

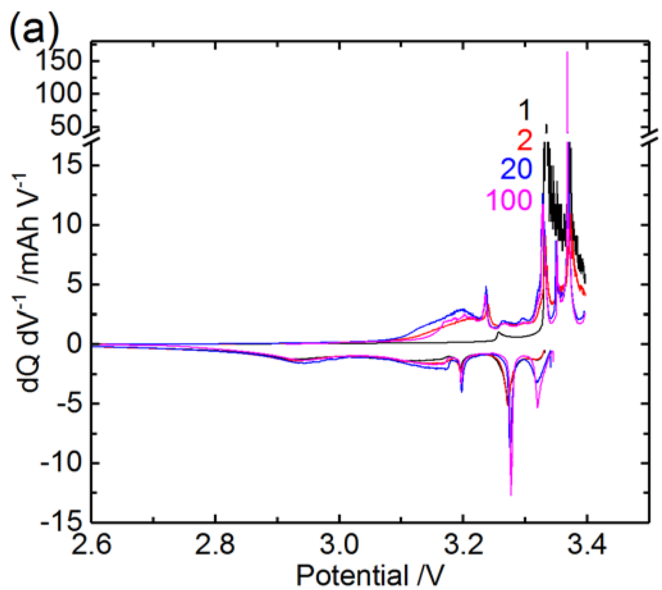

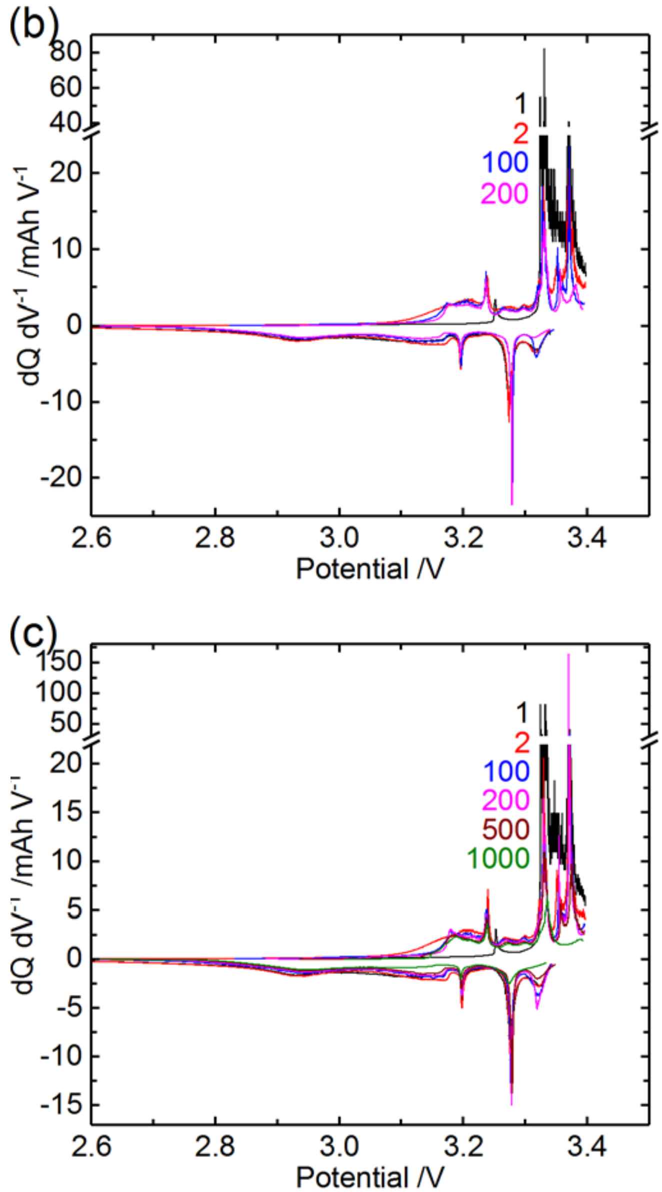

Fig. S5. Differential capacity dQ dV^{-1} plots for Si-graphite cycled against a $LiFePO_4$ reference electrode at (a) C/10, (b) C/5, and (c) 1C. In (b) and (c) the first and last 3 cycles of each set of 100 cycles were performed at C/10 while the intermediate cycles were performed at C/5 and 1C, respectively. At C/10 100 cycles were collected, while 200 and 1000 cycles were collected at C/5 and 1C, respectively.

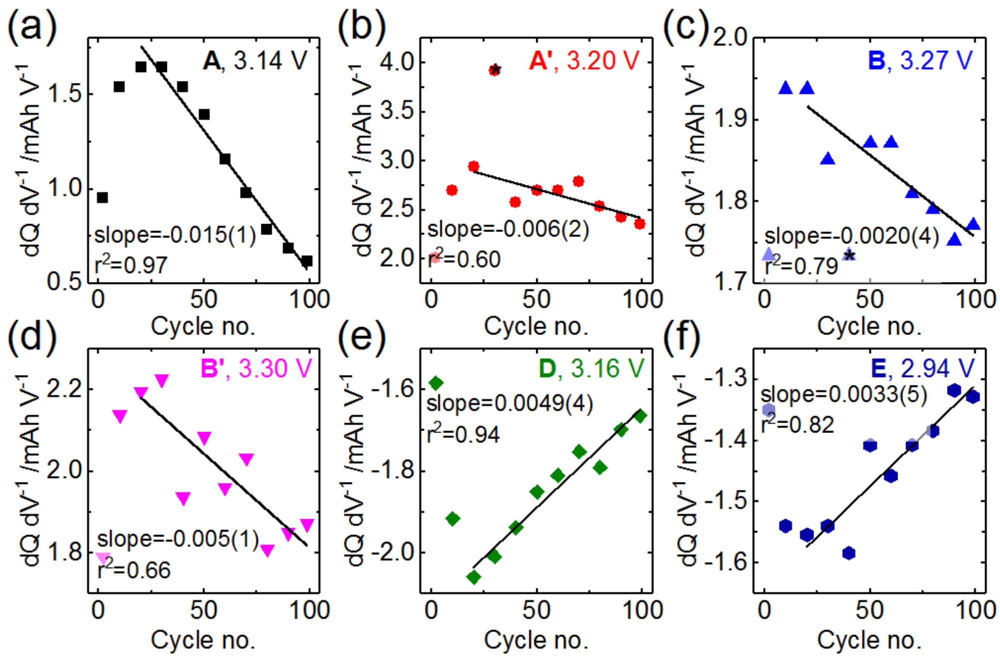

Fig. S6. Value of dQ dV^{-1} at various potentials on lithiation (a-d) and delithiation (e-f) with respect to cycle number for 15%Si-graphite cycled against a $LiFePO_4$ reference electrode at C/10. The linear fit shown was taken between cycle 20 and cycle 100. In (b) and (c) the data point marked with * was treated as an outlier and excluded from the fit.

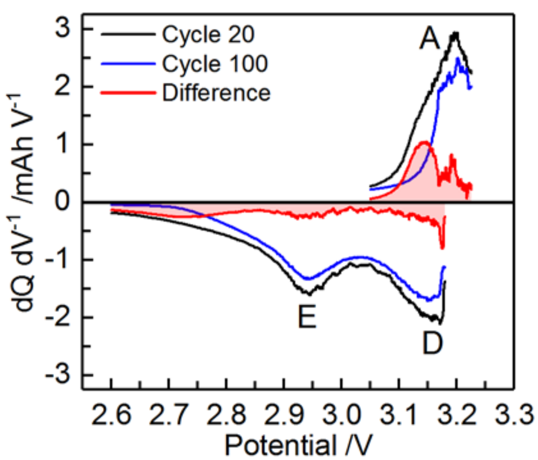

Fig. S7. Differential capacity dQ dV^{-1} and intensity separation of the dQ dV^{-1} signal between cycle 20 and cycle 100 at C/10 for the isolated Si processes (A, D and E in Fig. 2), *i.e.*, those not overlapped by graphite processes.

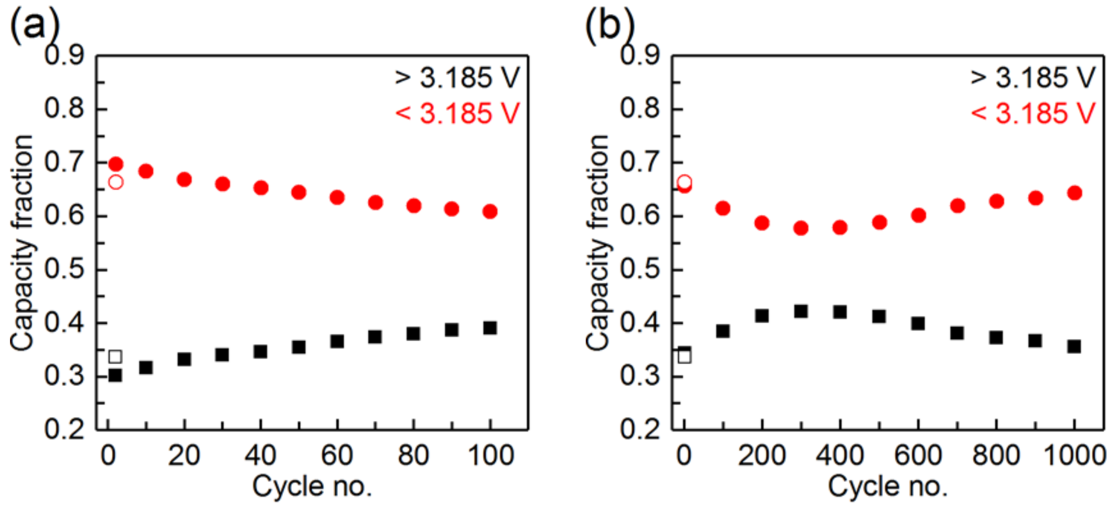

Fig. S8. Fraction of capacity above and below 3.185 V on delithiation with cycle number for 15%Si-graphite cycled against a $LiFePO_4$ reference electrode at (a) C/10, and (b) 1C. In (b) the first and last 3 cycles of each set of 100 cycles were performed at C/10. At C/10 100 cycles were collected, while 1000 cycles were collected at 1C. The open data points at cycle 1 show the theoretical fraction of capacity for the graphite (black) and Si (red) components of the blended Si-graphite laminate, assuming full utilization of each component, and a theoretical capacity of 372 mAh g^{-1} and 3572 mAh g^{-1} for graphite and Si, respectively. It appears that the fraction of capacity above and below 3.185 V is a good approximation of the capacity delivered from the individual graphite and Si components, respectively. Therefore, the trends reveal the changes in the fraction of capacity delivered from graphite and Si in the blended electrode with extended cycling.

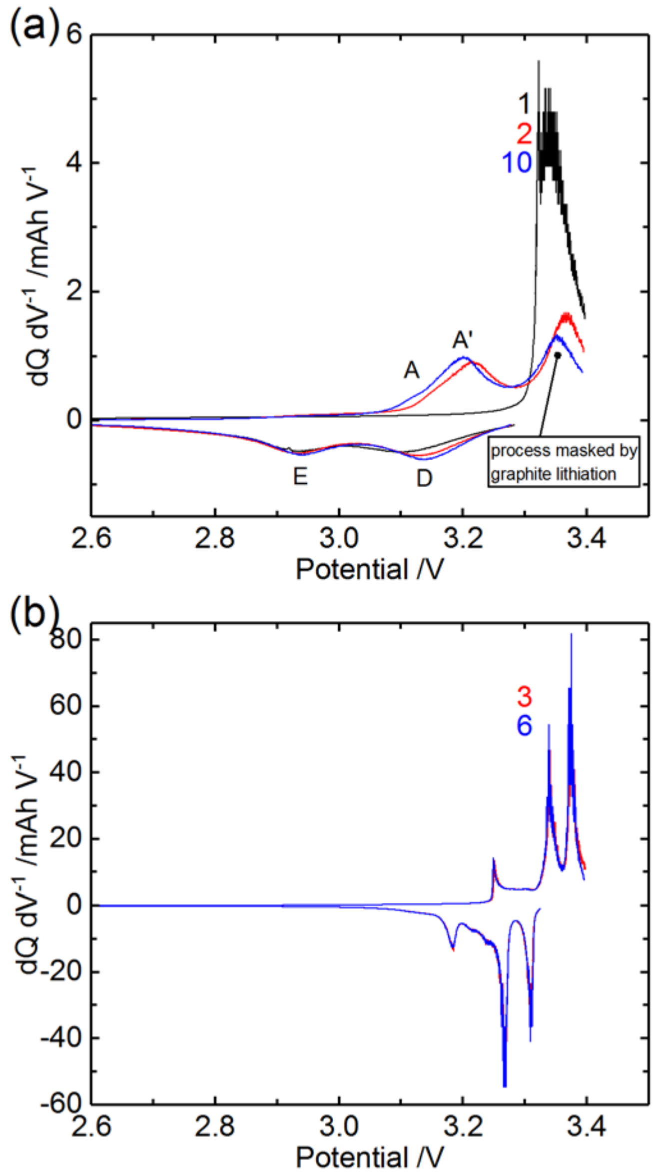

Fig. S9. Differential capacity dQ dV^{-1} plots for (a) Si-only and (b) graphite-only cycled against a $LiFePO_4$ reference electrode at C/10 with the cycle number indicated. These plots are used, together with relevant literature, to assign graphite and Si related process for the Si-graphite composite electrode in Fig. 2. For direct comparison, Si processes marked with letters in Fig. 2 are similarly marked in (a). The second lithiation process in (a) is unmarked since this process is masked by graphite lithiation processes in Fig. 2. Notably, processes C is not observed in either the Si-only or the graphite-only differential potential plots, supporting our hypothesis that it arises from some Si-graphite interaction. Graphite processes shown in (b) are consistent with those marked with asterisks in Fig. 2.

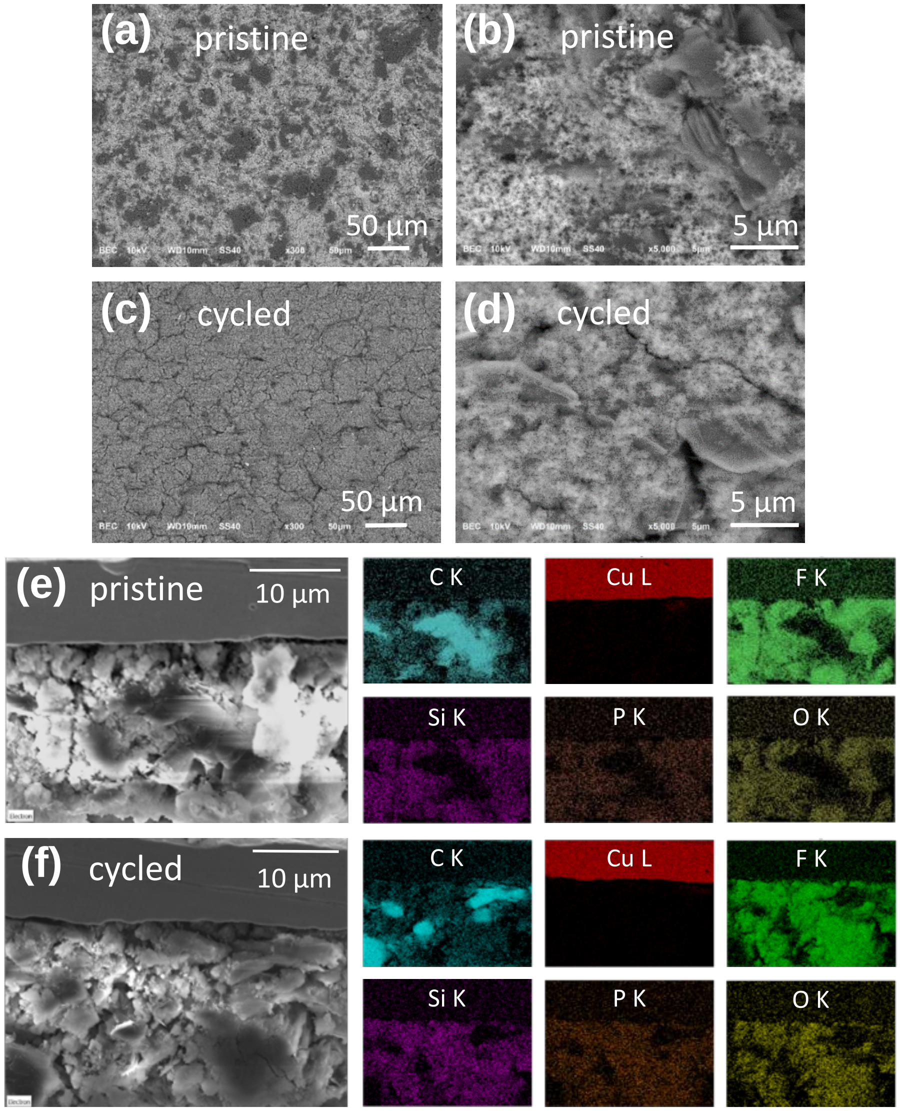

Fig. S10. SEM images of the pristine 15%Si-graphite electrode (a, b, e) and after extended cycling (c, d, f). Figures a-d were collected using a BEC detector and the contrast clearly differentiates the graphite (darker) and Si (lighter) domains in the pristine electrode (a), while the segregation is not as evident after 500 cycles at a 1C rate (c). SEM of the pristine (e) and cycled (f) electrode cross-section and their corresponding elemental mapping (C, Cu, F, Si, P and O) obtained using the EDX detector. These images highlight that sizeable graphite (carbon) domains are still present in both the pristine and cycled electrode, 100 cycles at a C/5 rate.

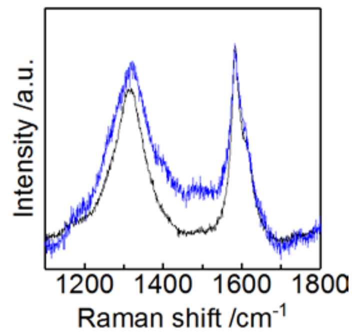

Fig. S11. Normalized averaged Raman spectra in the region 1100-1800 cm^{-1} for the pristine 15%Si-graphite electrode (black) and after extended cycling (blue). Data are normalized to the intensity of the 1583 cm^{-1} peak to illustrate the increase in the disordered carbon at the expense of ordered carbon.